Acta Crystallographica Section D
Biological Crystallography
ISSN 0907-4449

Crystallization and rhenium MAD phasing of the acyl-homoserinelactone synthase EsaI

William T. Watson,[a] Frank V. Murphy IV,[a] Ty A. Gould,[a] Per Jambeck,[b] Dale L. Val,[c] John E. Cronan Jr,[c] Susanne Beck von Bodman[d] and Mair E. A. Churchill[a,b]*

[a]Department of Pharmacology, The University of Colorado Health Sciences Center, 4200 East Ninth Avenue, Denver, CO 80262, USA, [b]Cell and Structural Biology Department, University of Illinois at Urbana-Champaign, USA, [c]Departments of Microbiology and Biochemistry, University of Illinois at Urbana-Champaign, USA, and [d]Departments of Plant Science and Molecular and Cell Biology, University of Connecticut, 302 B Ag. Biotech, Storrs, CT 06269-4163, USA

Correspondence e-mail: mair.churchill@uchsc.edu

Received 25 May 2001
Accepted 6 September 2001

PDB Reference: acyl-homoserinelactone synthase EsaI–rhenate complex, 1k4j.

Acyl-homoserine-L-lactones (AHLs) are diffusible chemical signals that are required for virulence of many Gram-negative bacteria. AHLs are produced by AHL synthases from two substrates, *S*-adenosyl-L-methionine and acyl-acyl carrier protein. The AHL synthase EsaI, which is homologous to the AHL synthases from other pathogenic bacterial species, has been crystallized in the primitive tetragonal space group $P4_3$, with unit-cell parameters $a = b = 66.40$, $c = 47.33$ Å. The structure was solved by multiple-wavelength anomalous diffraction with a novel use of the rhenium anomalous signal. The rhenium-containing structure has been refined to a resolution of 2.5 Å and the perrhenate ion binding sites and liganding residues have been identified.

1. Introduction

Acyl-homoserine-L-lactones (AHLs) act as bacterial pheromones that allow the bacterium to sense the cell density of its neighbors and to decisively control gene expression when a particular concentration or a 'quorum' of cells is reached (reviewed in De Kievit & Iglewski, 2000; Fuqua & Eberhard, 1999; Parsek & Greenberg, 2000). Highly similar quorum-sensing systems are employed by over 30 Gram-negative bacterial species and are essential for a wide variety of phenotypes including biofilm formation and virulence-factor production (Costerton *et al.*, 1999; Fuqua *et al.*, 1994). Biofilms that accompany many chronic infections are colonies encased in polysaccharide matrices that are resistant to both antimicrobials and host immune cells (Davies *et al.*, 1998; De Kievit & Iglewski, 1999; Parsek & Greenberg, 1999). The quorum-sensing system is composed of an AHL signal produced by the AHL synthase and a transcriptional response regulator (reviewed in Fuqua *et al.*, 1994; Fuqua & Greenberg, 1998; Parsek & Greenberg, 2000; Winans, 1988). In most cases, inactive mutants of either type of quorum-sensing regulator leads to the loss of the controlled phenotype (Rumbaugh *et al.*, 1999), which suggests that inactivating the quorum-sensing regulators will be an effective way to inhibit bacterial quorum-sensing communication and pathogenesis.

The sweetcorn pathogen *Pantoea stewartii* ssp. *stewartii* synthesizes an extracellular polysaccharide matrix required for virulence in a quorum-sensing controlled manner (Beck von Bodman & Farrand, 1995; Beck von Bodman *et al.*, 1998). Crystallographic studies of the *P. stewartii* AHL synthase (EsaI) were initiated to obtain the first high-resolution view of this novel class of enzymes and to facilitate structure-based antimicrobial design. Solution of the EsaI structure from ammonium perrhenate soaked crystals shows that use of rhenium can be an effective approach for MAD phasing. Characterization of the perrhenate-binding sites provides insight into the mechanism of incorporation for this compound.

2. Materials and methods

2.1. Overexpression and purification

The gene encoding EsaI was subcloned into pET14b by PCR from the parent plasmid pSVB5-18, which is a pBluescriptSK+ derivative that carries the native *esa*I/*esa*R gene cluster (Beck von Bodman & Farrand, 1995). Primers used to amplify the EsaI coding sequence for subcloning into the *Nco*I/*Xho*I-digested pET14b vector, where the *Nco*I site reconstitutes the ATG initiation codon, are 5′-CTCTCGGAAT**CATATG**CTTGAACTG-3′ and 5′-CTCGTAGTAGAAC**CTCGAG**TTAT-CAGACC-3′. Digestion of the PCR product with *Nco*I and *Xho*I allowed ligation of the EsaI coding sequence into the similarly digested pET14b vector. The final plasmid was verified by DNA sequencing.

EsaI was overexpressed in *Escherichia coli* strain BL21(DE3) (Novagen; Studier *et al.*, 1990) grown in a fermenter in ampicillin-containing minimal media with lactose induction [0.2%(*w*/*v*)] as described previously

(Hoffman *et al.*, 1995). The cell pellet was stored at 193 K. The frozen cell paste (60 g) was thawed on ice and resuspended in 200 ml of PBS (50 m*M* sodium/potassium phosphate and 0.3 *M* NaCl pH 8.0) by vigorous pipetting and shaking. Cells were lysed by incubating in 0.75 mg ml^{-1} lysozyme, 100 m*M* benzamidine and 10 m*M* leupeptin on ice for 30 min, followed by sonication for 10 min at 30 W on a 50% duty cycle. Insoluble cellular debris was removed by centrifugation at 15 000*g*. The supernatant was adjusted to pH 8.0 with NaOH and then incubated with mixing in a 1 ml bed volume of washed Ni-NTA resin (Qiagen) at 277 K for 1 h. The EsaI-bound resin was washed three times with greater than ten bed volumes of 50 m*M* NaH_2PO_4 pH 8.0, 0.3 *M* NaCl, 10 m*M* imidazole and packed into a column. The protein was eluted with an imidazole gradient of 10–250 m*M* imidazole and fractions containing EsaI were pooled and dialyzed at 100-fold dilution three times into 20 m*M* HEPES pH 7.5, 0.3 *M* NaCl and 10 m*M* DTT. After dialysis to remove the imidazole and salts, the EsaI protein is approximately 95% pure by Coomassie-stained SDS–PAGE and mass spectrometry (data not shown). The purified protein was stored by flash-freezing in liquid N_2 and thawed on ice prior to crystallization trials.

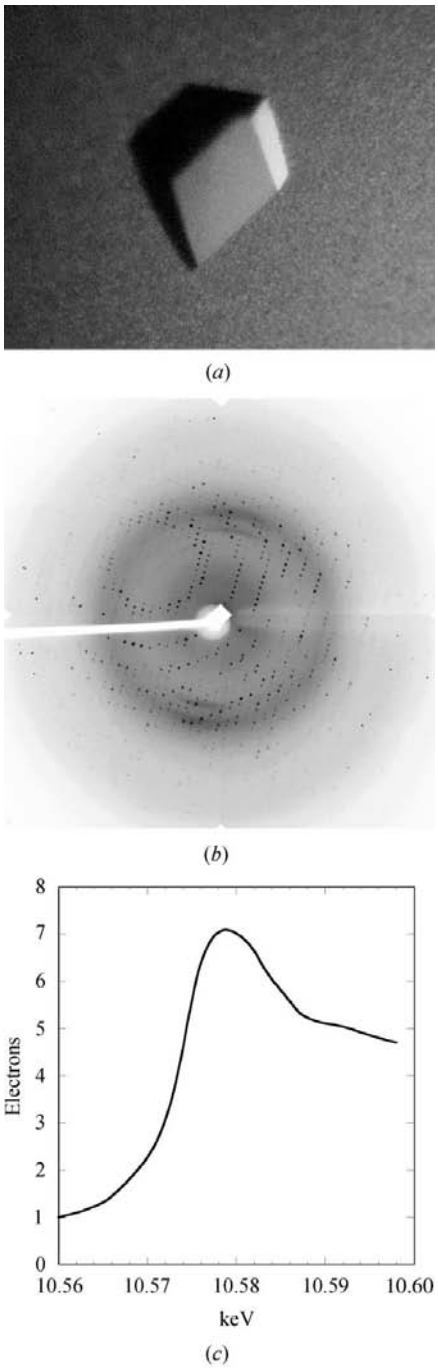

Figure 1
Crystallographic analysis of EsaI crystals. (*a*) Typical native chunky plate crystals of EsaI with dimensions 0.4 × 0.4 × 0.2 mm. (*b*) Diffraction image from a native EsaI crystal. The image was collected under cryocooling conditions (93 K nitrogen stream) for 30 s with an oscillation of 1°. Reflections are visible to the edge of the Quantum4 CCD area detector (Advanced Photon Source beamline 14C), which is 1.8 Å resolution at a distance of 100 mm. (*c*) Plot of fluorescence scan showing the rhenium absorption edge.

2.2. Crystallization

The EsaI protein was concentrated to approximately 6 mg ml^{-1} as assessed by UV absorbance scan (extinction coefficient at 280 nm = 33 200). Purified EsaI and all crystallization solutions were sterile-filtered to remove contaminants. Optimal crystallization conditions are 0.1 *M* MES pH 6.1, 14% PEG 4000, 6% 2-propanol, 0.03% β-mercaptoethanol, 10 m*M* EDTA, 0.5% NaN_3. The addition of melted agarose at 313 K to the drop at a final concentration of 0.01% reduced the formation of a protein skin on the drop surface (Robert *et al.*, 1992). Typical crystals grew by vapor diffusion at 291 K in 3 d as house-shaped blocks of 200 × 200 × 100 µm. The perrhenate-soaked crystal was prepared by adding ammonium perrhenate to the drop at a final concentration of approximately 27 m*M*, followed by overnight soaking before freezing.

2.3. Data collection and analysis

Multiple-wavelength anomalous diffraction data were collected on a single ammonium perrhenate soaked EsaI crystal at Brookhaven National Synchrotron Light Source on beamline X12C. Cryocooling required that the crystal be immersed in paraffin oil for several seconds prior to mounting and freezing in the 113 K nitrogen stream to reduce ice and damage to the crystal from evaporation of the volatile mother liquor. The MAD data were collected with a crystal-to-image plate distance of 100 mm and oscillations of 1.0° for 45 s on the Brandeis-B4 detector. The rhenium L_{III} absorption edge was measured by a scan of the X-ray fluorescence over the expected range of rhenium absorption, approximately 1.14–1.19 Å. Data were collected at four wavelengths using the 'Friedel flip' method of MAD data collection (R. Sweet, personal communication). This method collects data at each wavelength for a 15° sweep followed directly by the same sweep + 180° to obtain the best coverage of Friedel pairs before moving on to the next sweep in the oscillation range of the 72° of reciprocal space required to complete the data set. The Re absorption edge was measured at the beginning of each sweep.

Images were autoindexed and the data processed and reduced with the programs *DENZO* and *SCALEPACK* implemented in *HKL* (Otwinowski & Minor, 1997). The intensities were then converted to amplitudes using the *TRUNCATE* program in the *CCP*4 suite of crystallographic programs (Collaborative Computational Project, Number 4, 1994). Resolution shells that did not meet the stringent criteria for data quality of $R_{sym} < 0.20$ and $I/\sigma > 2$ were not included, which results in different maximum resolutions for the different wavelengths.

2.4. MAD phasing and structure determination

Initial phases were obtained by analysis of the anomalous signal produced from Re atoms bound in the native EsaI crystal. Heavy-atom positions for five perrhenate ions were identified using the program *SOLVE*, which produced initial phases and electron-density maps (Terwilliger & Berendzen, 1999). The solvent content of the crystal was estimated to be approximately 37.5%, consistent with one molecule per asymmetric unit (Brunger *et al.*, 1998). Density modification with the program *RESOLVE* (Terwilliger, 2000) improved the maps sufficiently to build much of the initial model using *O* (Jones *et al.*, 1991). Maximum-likelihood refinement procedures, including energy minimization with a bulk-solvent correction, simulated annealing and individual *B*-factor refinement, implemented in *CNS* were used to improve phase estimates and electron-density calculations (Brunger *et al.*, 1998). Before the final

refinement round of this model, two additional perrhenate ions and water molecules were incorporated based on the size and environment of the largest peaks in $F_o - F_c$ maps calculated after initial model refinement. These putative perrhenates, 406 and 407, were not identified from the rhenium anomalous signal and their inclusion did not substantially improve model refinement.

3. Structural analysis

PROCHECK and *ANALYSE* (*CNS*) programs were used to evaluate the stereochemistry of the protein model (Brunger *et al.*, 1998; Laskowski, 1993). Perrhenate-binding sites identified by *SOLVE* were examined by inspection of difference Fourier maps and composite simulated-annealing omit maps ($2F_o - F_c$) using *O*. The sites were further characterized by electrostatic surface analysis using *GRASP* (Nicholls *et al.*, 1993) and the program *CONTACTS* from the *CCP*4 suite of programs (Collaborative Computational Project, Number 4, 1994). Contacts within the range of the sum of the two van der Waals radii plus 0.5 Å are called van der Waals contacts. Contacts within the hydrogen-bond distance of 3.4 Å between donor and acceptor atoms and those ionic interactions within 4.5 Å are described as electrostatic interactions.

4. Crystallization and X-ray crystallographic analysis

The 229 amino-acid EsaI protein included an N-terminal His_6 tag, facilitating isolation and purification using nickel-agarose affinity chromatography. Small crystals of EsaI were obtained by vapor diffusion using a sparse-matrix approach (Jancarik & Kim, 1991) implemented in the Hampton Scientific crystal screen. Crystals were improved by extensive optimization, including the use of agarose gel in the protein drop and MES as the buffer (Fig. 1*a*). Crystals form in the tetragonal space group $P4_3$, with unit-cell parameters 66.40 × 66.40 × 47.33 Å and one molecule per asymmetric unit. The solvent content of this crystal is calculated to be between 36.3–38.7% and the Matthews coefficient is 2.006 $Å^3\ Da^{-1}$ (Brunger *et al.*, 1998). The native crystals can diffract to at least 1.8 Å, as observed at the Advanced Photon Source beamline 14C (Fig. 1*b*).

Extensive efforts to solve the EsaI structure focused on MIR and MAD methods. Multiple isomorphous replacement (MIR) methods with ∼20 different compounds resulted in three derivatives of different qualities that were all non-isomorphous (gold, mercury and rhenium). Multiple-wavelength anomalous diffraction (MAD) methods (Hendrickson & Ogata, 1997) with selenomethionine incorporation failed because the selenium signal was not strong enough to locate Se atoms within the unit cell. Crystallographic structure determination by MAD requires heavy atoms with absorption edges within the available limits of variable synchrotron-radiation sources. By trying 15 such 'MAD-atom' containing compounds in crystal soaks (uranyl acetate, thimersol, PCMB, lead citrate, sodium orthovanadate, stannous chloride, methylmercury, mercuric acetate, ammonium cyanoaurate, bismuth chloride, iridium chloride, lead chloride, barium chloride, potassium osmate and ammonium perrhenate), a suitable derivative with high-quality diffraction was only obtained with ammonium perrhenate. Four wavelengths for MAD data were collected to 2.45 Å on synchrotron beamline X12C, NSLS, Brookhaven National Laboratory on the basis of X-ray fluorescence scans that identified peak and inflection energies (Fig. 1*c*). These data sets were processed, scaled and analyzed using *DENZO* and *SCALEPACK* (Table 1).

Initial phases were calculated using the program *SOLVE* in three space groups ($P4$, $P4_1$, $P4_3$) and with swapped anomalous data to account for potential space-group ambiguities. Five rhenium sites were identified in

Table 1
Data-collection and scattering-factor results.

Values in parentheses are for the highest resolution shell.

	λ_1	λ_2	λ_3	λ_4
Wavelength (Å)	1.14	1.1724	1.1719	1.19
Resolution range (Å)	30–2.5 (2.6–2.5)	30–2.7 (2.8–2.7)	30–2.7 (2.8–2.7)	30–2.5 (2.6–2.5)
Completeness (%)	97.0 (98.1)	97.6 (98.7)	97.7 (98.9)	96.9 (99.5)
R_{sym}† (%)	4.2 (17.5)	4.8 (14.8)	5.7 (17.6)	3.3 (17.9)
$\langle I/\sigma \rangle$	20.9 (4.7)	11.5 (6.3)	17.7 (3.8)	26.6 (5.2)
Observed reflections	32922	28546	28071	36442
Unique reflections	7283	5764	5772	7313
f' initial	−9.88	−14.3	−13.7	−12.9
f'' initial	9.68	8.70	9.50	3.90
f' final	−8.72	−17.68	−11.43	−9.57
f'' final	6.43	9.33	11.49	2.76

† R_{sym} (on intensity) = $\sum\sum |I(h)_i - \langle I(h)\rangle| / \sum\sum I(h)_i$, where $I(h)_i$ is the observed intensity and $\langle I(h)\rangle$ is the mean intensity of reflection h over all measurements of $I(h)$.

Table 2
MAD phasing and structure statistics.

Phasing and refinement statistics	λ_1
Figure of merit after phasing (*SOLVE*)	0.33
Figure of merit after solvent flattening (*RESOLVE*)	0.57
Overall *SOLVE Z* score	19.0
Resolution range (Å)	30–2.5 (2.59–2.50)
$R_{working}$† (90% of data)	21.2 (25.4)
R_{free}† (10% of data)	27.4 (29.6)
R.m.s. deviations from ideality	
Bond lengths (Å)	0.008
Bond angles (°)	1.98
Dihedrals (°)	23.8
Impropers (°)	0.84
No. of atoms	
Protein	1515
Perrhenate	35
Water molecules	21
B average ($Å^2$)	52.5

† $R = \sum ||F_o| - |F_c|| / \sum |F_o|$; R_{free} was calculated with an excluded set of reflections.

Table 3
Perrhenate–protein contacts.

ReO_4 site	van der Waals	Electrostatic
1, Occ† = 0.26, *B*† = 44, peak height‡ = 5.99	Pro117, Ile118, Ser119, Gln120, Arg193	Pro117 O, Ser119 N, Ser119 O^{γ}, Gln120 N, Arg193 NH1
2, Occ† = 0.54, *B*† = 49, peak height‡ = 9.37	His84, Cys85, Lys161, Ala163, Phe164	Cys85 O, Lys161 N^{ζ}, Phe164 N, Phe164 O
3, Occ† = 0.49, *B*† = 53, peak height‡ = 8.43	Re407, Phe101, Ile141, Val142, Ser143, Met146	Ser143 N, Ser143 O^{γ}, Phe101 O, Phe101 N, Ile141 O
4, Occ† = 0.37, *B*† = 57, peak height‡ = 5.77	Phe101, Val103, Lys105, Ser119, Ile149	Ser119 O^{γ}, Lys105 N^{ζ}, Re401
5, Occ† = 0.27, *B*† = 60, peak height‡ = 4.09	Glu114, His115, Tyr116, Pro117, Arg193, Thr194	Glu114 O, His115 O, Tyr116 N, Arg193 O, Thr194 N
6, Occ§ = 0.15, *B*§ = 64, peak height‡ = 3.48	Gly51, Arg53, Phe69, Ser71, Thr70, Gly95, Thr96, Trp129, Tyr135	Gly51 O, Ser71 O^{γ}, Thr96 $O^{\gamma 1}$, Tyr135 OH
7, Occ§ = 0.15, *B*§ = 63, peak height‡ = 3.28	Met77, Phe82, Ile141, Val142, Leu165, Ile171	Ile141 O, Ser143 N, Val142 O, Re403

† Occupancy and *B* factor determined by *SOLVE*. ‡ Peak height determined after refinement with *CNS* from a $2F_o - F_c$ map. § Occupancy and *B* factor determined after refinement with *CNS*.

the $P4_3$ space group with swapped anomalous data giving a Z score of 19. Significant refinement of the scattering factors f' and f'', compared with the values expected from Sasaki tables (in *SHARP*; de La Fortelle & Bricogne, 1997) for the Re atom (Table 1), may indicate the difference in chemical environment of the rhenium in the perrhenate ion (ReO_4) and the protein. The maximum-likelihood density-modification program *RESOLVE* (Terwilliger, 2000) improved the modest quality phases, figure of merit 0.33, from *SOLVE* and produced a clearly interpretable electron-density map with a figure of merit of 0.57 (Table 2). The chain was traced and the model containing the perrhenates was partially refined using *CNS* (Brunger *et al.*, 1998) (Table 2). A section of the map shows the shape of the electron density and interacting residues of four of the perrhenate ions (Fig. 2*a*).

The perrhenate MAD signal allowed identification of the positions of the bound perrhenate and subsequent initial phase estimates permitted the EsaI structure to be determined to 2.5 Å resolution. There are no reports of protein structures containing bound perrhenate, although it was expected that the ion would occupy slightly electropositive sites in the protein. The contacting residues within van der Waals contact distance and those residues that have either hydrogen bonding or electrostatic interactions are shown in Table 3. The occupancies of the ions are relatively low and the ions have relatively high B factors. Therefore, it is likely that the ions do not occupy all of the sites simultaneously, which also explains the high average B factor of the overall model. The ReO_4 ions interact mainly with EsaI amide, amine, guanidinium, hydroxyl and carbonyl groups (Fig. 2 and Table 3). The ions bind in surface clefts that are slightly electropositive relative to the majority of the protein's surface, as seen in an electrostatic surface representation of EsaI showing five of the perrhenate sites (Fig. 2*b*). In contrast to the front view, the reverse side of the protein is smoother and is more negatively charged and has no perrhenate-binding sites.

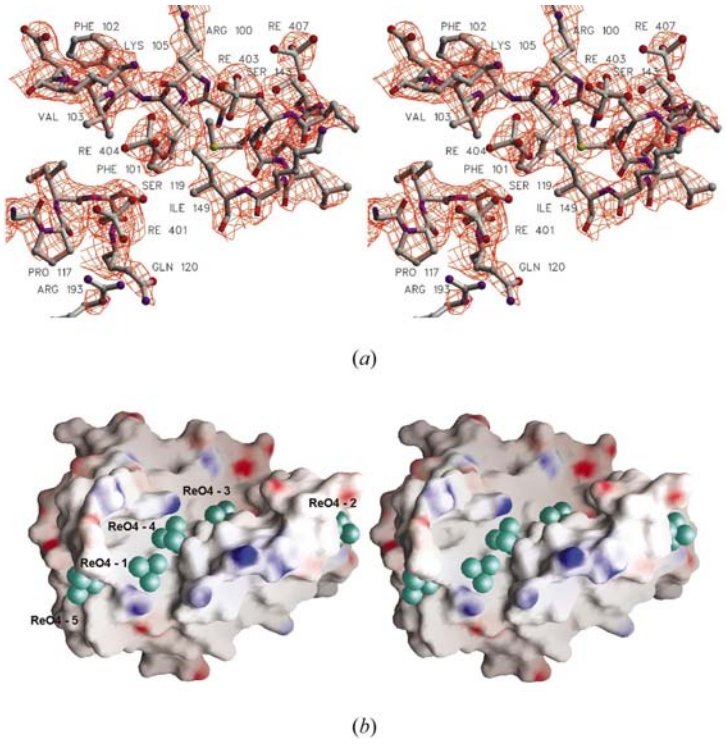

Figure 2
Perrhenate binding sites. (*a*) A stereoview of a simulated-annealing composite omit map ($2F_o - F_c$) contoured at 1σ illustrates the environment of four rhenium ions in the protein. The figure was generated using *SETOR* (Evans, 1993) and *Photoshop* (Adobe). (*b*) A *GRASP* surface representation of EsaI in stereoview colored according to the calculated electrostatic potential with the most electronegative regions colored in red, and the most electropositive in blue (Nicholls *et al.*, 1993). The five positively identified perrhanate ions, based on their anomalous signal by *SOLVE*, are shown as green spheres.

5. Conclusions

A novel enzyme that is important for regulation of bacterial pathogenesis in *P. stewartii* ssp. *stewartii* has been crystallized and diffraction data to 1.8 Å have been collected. The MAD signal from a rhenium-soaked crystal was used to solve the structure, after other methods including selenomethionine MAD and MIR had failed. The perrhenate ions bind in a hydrophilic and slightly electropositive cleft in the protein near the enzyme active site. Interestingly, the majority of the electrostatic interactions between the protein and the perrhenate ions are with basic nitrogen species and serine hydroxyl O atoms.

We thank Bob Sweet and members of the X12C beamline at NSLS for advice on MAD data collection, Eric Johnson for running the fermentor for both the regular and the Se-Met fermentations and Janet Klass for reading the manuscript. The UCHSC Biomolecular X-ray Crystallography Facility was supported in part by funding from The Howard Hughes Medical Institute. We acknowledge support from the NIH (MEAC), American Heart Association (Established Investigator Grant to MEAC) and The Cystic Fibrosis Foundation (Predoctoral Research Award to WTW).

References

Beck von Bodman, S. & Farrand, S. K. (1995). *J. Bacteriol.* **177**, 5000–5008.
Beck von Bodman, S., Majerczak, D. R. & Coplin, D. L. (1998). *Proc. Natl Acad. Sci. USA*, **95**, 7687–7692.
Brunger, A. T., Adams, P. D., Clore, G. M., DeLano, W. L., Gros, P., Grosse-Kunstleve, R. W., Jiang, J.-S., Kuszewski, J., Nilges, M., Pannu, N. S., Read, R. J., Rice, L. M., Simonson, T. & Warren, G. L. (1998). *Acta Cryst.* D**54**, 905–921.
Collaborative Computational Project, Number 4 (1994). *Acta Cryst.* D**50**, 760–763.
Costerton, J. W., Stewart, P. S. & Greenberg, E. P. (1999). *Science*, **284**, 1318–1322.
Davies, D. G., Parsek, M. R., Pearson, J. P., Iglewski, B. H., Costerton, J. W. & Greenberg, E. P. (1998). *Science*, **280**, 295–298.
De Kievit, T. R. & Iglewski, B. H. (1999). *Methods Enzymol.* **310**, 117–128.
De Kievit, T. R. & Iglewski, B. H. (2000). *Infect. Immun.* **68**, 4839–4849.
Evans, S. (1993). *J. Mol. Graph.* **11**, 134–138.
Fuqua, C. & Eberhard, A. (1999). *Cell–Cell Communication in Bacteria*, edited by G. Dunny & S. C. Winans, pp. 211–230. AMS Press.
Fuqua, W. C. & Greenberg, E. P. (1998). *Curr. Opin. Microbiol.* **1**, 183–189.
Fuqua, W. C., Winans, S. C. & Greenberg, E. P. (1994). *J. Bacteriol.* **176**, 269–275.
Hendrickson, W. A. & Ogata, C. M. (1997). *Methods Enzymol.* **276**, 494–522.
Hoffman, B. J., Broadwater, J. A., Johnson, P., Harper, J., Fox, B. G. & Kenealy, W. R. (1995). *Protein Expr. Purif.* **6**, 646–654.
Jancarik, J. & Kim, S.-H. (1991). *J. Appl. Cryst.* **24**, 409–411.
Jones, T. A., Zou, J. Y., Cowan, S. W. & Kjeldgaard, M. (1991). *Acta Cryst.* A**47**, 110–119.

La Fortelle, E. de & Bricogne, G. (1997). *Methods Enzymol.* **276**, 472–494.
Laskowski, R. A. (1993). *J. Appl. Cryst.* **26**, 283–291.
Nicholls, A., Bharadwaj, R. & Honig, B. (1993). *Biophys. J.* **64**, A166.
Otwinowski, Z. & Minor, W. (1997). *Methods Enzymol.* **276**, 307–326.
Parsek, M. R. & Greenberg, E. P. (1999). *Methods Enzymol.* **310**, 43–55.
Parsek, M. R. & Greenberg, E. P. (2000). *Proc. Natl Acad. Sci. USA*, **97**, 8789–8793.
Robert, M. C., Provost, K. & Lefaucheux, F. (1992). *Crystallization of Nucleic Acids and Proteins: A Practical Approach*, edited by A. Ducruix & R. Giegé, pp. 127–143. Oxford University Press.
Rumbaugh, K. P., Griswold, J. A., Iglewski, B. H. & Hamood, A. N. (1999). *Infect. Immun.* **67**, 5853–5862.
Studier, F. W., Rosenberg, A. H., Dunn, J. J. & Dubendorff, J. W. (1990). *Methods Enzymol.* **185**, 60–89.
Terwilliger, T. C. & Berendzen, J. (1999). *Acta Cryst.* D**55**, 849–861.
Terwilliger, T. C. (2000). *Acta Cryst.* D**56**, 965–972.
Winans, S. C. (1988). *Trends Mircobiol.* **6**, 382–383.